Author/s:
Jenkins, ZA;Macharg, A;Chang, CY;van Kogelenberg, M;Morgan, T;Frentz, S;Wei, W;Pilch, J;Hannibal, M;Foulds, N;McGillivray, G;Leventer, RJ;García-Miñaúr, S;Sugito, S;Nightingale, S;Markie, DM;Dudding, T;Kapur, RP;Robertson, SP

Title:
Differential regulation of two FLNA transcripts explains some of the phenotypic heterogeneity in the loss-of-function filaminopathies

Date:
2018-01-01

Citation:
Jenkins, Z. A., Macharg, A., Chang, C. Y., van Kogelenberg, M., Morgan, T., Frentz, S., Wei, W., Pilch, J., Hannibal, M., Foulds, N., McGillivray, G., Leventer, R. J., García-Miñaúr, S., Sugito, S., Nightingale, S., Markie, D. M., Dudding, T., Kapur, R. P. & Robertson, S. P. (2018). Differential regulation of two FLNA transcripts explains some of the phenotypic heterogeneity in the loss-of-function filaminopathies. Human Mutation, 39 (1), pp.103-113. https://doi.org/10.1002/humu.23355.

Differential regulation of two *FLNA* transcripts explains some of the phenotypic heterogeneity in the loss-of-function filaminopathies

Zandra A Jenkins[1], Alison Macharg[1], Cheng-Yee Chang[1], Margriet van Kogelenberg[1], Tim Morgan[1], Sophia Frentz[1], Wenhua Wei[1], Jacek Pilch[2], Mark Hannibal[3], Nicola Foulds[4], George McGillivray[5], Richard J Leventer[6], Sixto García-Miñaúr[7], Stuart Sugito[8], Scott Nightingale[9], David M Markie[10], Tracy Dudding[8], Raj P Kapur[11], Stephen P Robertson[1]

Affiliations

1. Department of Women's and Children's Health, Dunedin School of Medicine, University of Otago, Dunedin, New Zealand

2. Department of Child Neurology, Medical University of Silesia, Katowice, Poland

3. Department of Medical Genetics, Seattle Children's Hospital, Seattle, WA, USA

4. Wessex Regional Genetics Service, Southampton, UK

5. Victorian Clinical Genetics Service, Royal Children's Hospital, Melbourne, Australia

6. Department of Neurology, Royal Children's Hospital, Murdoch Childrens Research Institute and University of Melbourne, Department of Paediatrics, Melbourne, Australia

7. Department of Medical Genetics, Hospital Universitario La Paz, Madrid, Spain

8. Hunter Genetics, Newcastle, Australia

9. University of Newcastle, GrowUpWell Priority Research Centre, UK

10. Department of Pathology, Dunedin School of Medicine, University of Otago, Dunedin, New Zealand

11. Department of Laboratories, Seattle Children's Hospital, Seattle, WA , USA

Corresponding Author

Stephen Robertson

stephen.robertson@otago.ac.nz

Phone +64 3 4797469

ABSTRACT

Loss-of-function mutations in the X-linked gene *FLNA* can lead to abnormal neuronal migration, vascular and cardiac defects and congenital intestinal pseudo-obstruction (CIPO), the latter characterised by anomalous intestinal smooth muscle layering. Survival in male hemizygotes for such mutations is dependent on retention of residual FLNA function but it is unclear why a subgroup of males with mutations in the 5' end of the gene can present with CIPO alone. Here we demonstrate evidence for the presence of two *FLNA* isoforms differing by 28 residues at the N-terminus initiated at ATG^{+1} and ATG^{+82}. A male with CIPO (c.18_19del) exclusively expressed FLNA ATG^{+82}, implicating the longer protein isoform (ATG^{+1}) in smooth muscle development. In contrast, mutations leading to reduction of both isoforms are associated with compound phenotypes affecting the brain, heart and intestine. RNA-seq data revealed three distinct transcription start sites, two of which produce a protein isoform utilising ATG^{+1} while the third utilises ATG^{+82}. Transcripts sponsoring translational initiation at ATG^{+1} predominate in intestinal smooth muscle, and are more abundant compared to the level measured in fibroblasts. Together these observations

describe a new mechanism of tissue-specific regulation of FLNA that could reflect the differing mechanical requirements of these cell types during development.

KEY WORDS

Filamin A

Chronic intestinal pseudo-obstruction

Periventricular neuronal heterotopia

Transcriptional regulation

1 INTRODUCTION

Mutations in the X-linked gene *FLNA* lead to a broad spectrum of clinical disorders – the filaminopathies. These clinical presentations have been grouped into two broad categories, loss-of-function filaminopathies, which are caused by mutations that lead to reduced or

absent expression, and gain-of-function filaminopathies, which are predominantly skeletal dysplasias and confer a pathogenic effect in the absence of an alteration in *FLNA* expression. Mutations leading to the latter conditions are clustered over the gene in positions denoting key functional domains of the protein (Robertson, 2005).

The phenotypic variability resulting from loss-of-function *FLNA* mutations is unsatisfactorily understood. These alleles result in phenotypes in females that have a disorder of neurogenesis, periventricular neuronal heterotopia (PVNH), as their prime presenting feature. PVNH is characterised radiologically by the formation of rests of grey matter along the surfaces of the lateral cerebral ventricles with the clinical consequences being seizures and occasionally, subtle learning disability (Parrini, et al., 2006). Males constitutively hemizygous for such alleles are typically lethally affected, with survival depending on the retention of some residual FLNA expression (Berrou, et al., 2017; Guerrini, et al., 2004; Oegema, et al., 2013; Sheen, et al., 2001). In a subset of these males, the clinical presentation is not only characterised by PVNH but also cardiovascular malformations and/or a specific form of intestinal dysmotility termed chronic intestinal pseudo-obstruction (CIPO) (Antonucci, et al., 2008; De Giorgio, et al., 2011). The mechanisms underlying this phenotypic variability are unexplained. This variability is particularly evident when comparing several reported families that segregate PVNH/CIPO (Clayton-Smith, et al., 2008; Hehr, et al., 2006; Kapur, et al., 2010; Oda, et al., 2016), in contrast to other families that

manifest a male-limited CIPO phenotype in which obligate female carriers are clinically unaffected (Gargiulo, et al., 2007; van der Werf, et al., 2012).

CIPO is characterised by abnormal bowel motility, presenting as intestinal obstruction in the absence of a mechanical lesion occluding the gut lumen (Antonucci, et al., 2008; De Giorgio, et al., 2011). Inability to maintain nutrition, body weight and growth through enteral feeding eventually leads to a reliance on parenteral nutritional supplementation (De Giorgio, et al., 2011). Pathologically, these infants manifest a short, dilated and frequently malrotated small intestine, with a microcolon being a variable co-attendant observation (Kapur, et al., 2010). Although, a neuropathy was considered to be the basis of the condition on the strength of an abnormal disposition of enteric neurons in the intramural intestinal plexuses, (Auricchio, et al., 1996), the subsequent demonstration of FLNA expression in normal enteric musculature and abnormal layering of the intestinal smooth muscle in males with loss-of-function *FLNA* mutations challenged this hypothesis, and established that the basis of the condition is more consistent with a myopathic etiology (Kapur, et al., 2010).

FLNA-associated CIPO, in addition to PVNH, has been described in several unrelated families, with the causative mutations being either, splice site variants (Hehr, et al., 2006), duplications (Clayton-Smith, et al., 2008; Kapur, et al., 2010) or deletions leading to exon

skipping (Oda, et al., 2016). Each of these mutations has the demonstrated or implied capacity to constitute a hypomorphic allele, suggesting that a PVNH/CIPO phenotype results from *FLNA* expression being reduced below a minimal threshold in the gut. This explanation is challenged, however, by several families with X-linked CIPO without attendant PVNH (Auricchio, et al., 1996; Gargiulo, et al., 2007; Kapur, et al., 2010; Royer, et al., 1974; van der Werf, et al., 2012). Auricchio et al (Auricchio, et al., 1996) first described a four-generation family with CIPO, with a 2 bp deletion in the 5' region of *FLNA* between two ATG codons (denoted here as ATG^{+1} and ATG^{+82}; Suppl. Fig. S1) separated by 28 codons (Gargiulo, et al., 2007) The male proband in this study had no demonstrable PVNH on MRI. A very similar family (van der Werf, et al.) also segregated a 2 bp deletion in this same region of *FLNA* in four affected males and carrier females (van der Werf, et al., 2012). Gargiulo et al. (Gargiulo, et al., 2007) proposed that both ATG codons could be recognised for translational initiation from a single cloned transcript but equivalent *in vivo* evidence was lacking. An alternative explanation is that *FLNA* specifies two proteins encoded by distinct transcripts with alternative 5' transcription start sites (TSS) and different N termini.

FLNA, plays diverse roles in the cell acting as a mechanical sensor (Huelsmann, et al., 2016; Lad, et al., 2007; Liu, et al., 2015; Nakamura, et al., 2014), a regulator of the cytoskeleton which influences cell shape and motility (Popowicz, et al., 2006), and a scaffolding hub for transmission of biochemical signalling pathways, which facilitate organogenesis in multiple

systems during embryonic development (Feng and Walsh, 2004; Robertson, et al., 2003). As a cytoskeletal protein, FLNA cross-links actin into either orthogonal networks or bundled stress fibres (Robertson, 2005; van der Flier and Sonnenberg, 2001) with the ratio of actin:filamin determining the relative stiffness of the cytoskeleton (Schmoller, et al., 2009).

Here, we investigate the regulation of FLNA expression through the lens of six families/individuals with loss-of-function mutations in *FLNA*. Through a comparative analysis of genotype and pathological phenotypes, we present evidence for differential transcriptional regulation of *FLNA*. These data indicate functional dependence in the gut on a transcript that is of low abundance in most tissues while cortical neurogenesis is possibly solely reliant on a more common, shorter transcript. These observations improve the understanding of genotype-phenotype predictions for *FLNA* variants and pose further questions addressing the role of FLNA protein isoforms, particularly during gastrointestinal development.

2 MATERIALS AND METHODS

2.1 Human subjects

Participants in this study were enrolled through physician-initiated referral and consented under a protocol approved by the Southern and Multi-regional Health and Disability Ethics Committee of New Zealand. Samples of ileum and colon small intestine samples were collected from consented cases under an approval granted by the Institutional Review Board of Seattle Children's Hospital, who were undergoing ileostomy or colostomy for unrelated indications, including necrotising enterocolitis.

2.2 Mutation screening

Genomic DNA from blood or skin fibroblasts was extracted using standard techniques. All exons and intron-exon boundaries were screened for mutations using bidirectional Sanger sequencing. All *FLNA* variants refer to Genbank accession number NM_001110556.1, and the protein coordinates to NP_001104026.1. RNA was extracted from the same sources using Nucleospin RNA Plus kit (Machery Nagel) and converted to cDNA with Superscript III (ThermoFisher). Copy number analysis was performed using a custom designed MLPA set that interrogates 19 sites within *FLNA* and its flanking regions and 2 autosomal control sites. Splicing analysis was performed on RNA extracted from fibroblast cells using semi-quantitative qRT-PCR primers spanning mutation-bearing exons followed by Sanger sequencing of products.

2.3 Immunohistochemistry

Surgical specimens and autopsy samples were fixed in formalin and embedded in paraffin for routine histology and immunohistochemistry. Immunostaining was performed on an automated platform (Benchmark XT, Ventana Medical Systems) using anti-FLNA aa1-27, 1:5000 (produced in rabbit using amino acids 1-27 as peptide antigen, Mimotopes Pty Ltd, Victoria, Australia) and rabbit anti-FLNA (Sigma HPA001115) at 1:100.

2.4 Immunofluorescence

Case 6 and two gender matched control fibroblast cell lines were grown on glass coverslips in DMEM, 10% FCS, penicillin 100U/ml and streptomycin 100 ug/ml, in 5% CO2 at 37^{o}C. Fixation was performed with 1% paraformaldehyde, followed by permeabilization and blocking with 7% FCS, 1% TritonX^{100} in PBS. Cells were incubated with antibodies diluted in PBS/7% FCS as indicated, FLNA antibody MAB1678 (Merck Millipore) 1:1000, anti GAPDH (Sigma G9545 1:500, followed by Alexa Fluor® 488 Goat Anti–Mouse, and Alexa Fluor® 594 Goat Anti–Rabbit at a dilution of 1:400, and finally stained with DAPI. Cells were visualized on an OLYMPUS BX53 using cellSense Dimension software. Comparative FLNA fluorescence was quantified using Fiji image analysis software; signal was normalized to background and GAPDH signal.

2.5 Western analysis

Case and gender-matched control EBV cell lines were grown in RPMI, 10%FCS, L-glutamine 2mM, and harvested by centrifugation. Cells were lysed in 1X Roche protease inhibitor cocktail, 1% TritonX100 in PBS at a concentration of 25mg/ml protein. Fibroblasts from subject cell lines and control gender-matched children were grown to 80% confluence and lysed as above in 25ul/cm2. All protein samples were denatured in 2% SDS, 10% Glycerol, 2.5% β-mercaptoethanol, 0.1% bromophenol blue, 50mM Tris.HCL pH 6.8, separated on a 7% SDS-PAGE gel, followed by transfer in Tris/Glycine buffer with 10% isopropanol to a nitrocellulose membrane for western blotting. Membranes were blocked in 5% milk/PBS, and probed with antibodies as follows, anti-FLNA MAB1678 1:5000, anti-FLNA aa1-27 1:250, and secondary antibodies Goat anti-mouse IRDYE 800CW and goat anti-rabbit IRDYE 680RD (Licor) at a dilution of 1:25000. Westerns were visualized on an Odyssey CLX and bands quantified using Image Studio software (Licor).

2.6 Cap Analysis Gene Expression (CAGE) - RNA sequencing

RNA was extracted from micro-dissected ileum and colon small intestine smooth muscle after homogenization in Trizol reagent and phase separation using the Nucleospin RNA Plus kit (Machery-Nagel), mixing the aqueous phase 3.5:1 with binding solution BS, and proceeding as per the protocol. CAGE RNA library construction and Illumina sequencing was

carried out by DNAFORM -Precision Gene Technologies, Japan. *FLNA* isoform expression and transcription start site (TSS) analysis was carried out using CAGEr software (Haberle, et al., 2015). Cluster analysis of TSS into regions initiated by independent promoters was performed using a maximal distance of 20bp and a read count threshold of 30.

2.7 FLNA mini-gene expression

FLNA mini-genes spanning the CHD1 domain, with unique 5'UTR's equivalent to TSS1, TSS2, and TSS3, and a FLNA wild type and FLNA variant (c.18_19del) were constructed spanning ATG+1 through to amino acid 110 (FLNA+1) in the pcDNA3.1V5/His vector. All plasmids were transfected into HEK293FT cells using a standard lipofectamine 2000 reverse transfection protocol. After 24 hours growth, cellular protein extracts were analysed by western blot as for fibroblast samples, using mouse anti-V5 1:3000 (Thermofisher) and rabbit anti-FLNA aa1-27 1:250, followed by Goat anti-mouse IRDYE 800CW and goat anti-rabbit IRDYE 680RD (Licor).

2.8 Analysis of FLNA amino acid conservation

Conservation of FLNA at an amino acid level was calculated for the following species, Homo sapiens, Mus musculus, Canis lupus, Bos taurus, Danio rerio, Xenopus tropicalis and Gallus

gallus, using the Clustal W tool, MegAlign™ (©1993-2017) version 9.1. DNASTAR. Madison, WI.

3 RESULTS

3.1 Clinical synopsis and mutation analysis

Five males (two being members of large extended kindreds) and one female with phenotypes previously linked to loss-of-function mutations at the *FLNA* locus (Table 1) were subject to further analysis after mutation screening uncovered instructive *FLNA* variants as the basis for their phenotypes. The phenotypes, spanning isolated PVNH or CIPO through to combinatorial CIPO/PVNH presentations, were selected for study to understand the mechanistic basis underpinning these different presentations. The reason for focusing on this male predominant subgroup of individuals was that the complicating factor introduced by X chromosome inactivation in female heterozygotes is eliminated in hemizygotes and the cognate phenotypes associated with *FLNA* variants can be less ambiguously studied.

Two cases (cases 1a and 1b, monozygotic twins; Fig. 1) had a compound presentation of PVNH and CIPO. These twins were born at term and in the neonatal period it became evident that a significant intestinal dysmotility disorder was present that evolved to require long-term parenteral nutrition. In addition, both boys developed respiratory symptoms, with bilateral bronchiectasis confirmed on CT scan. An MRI of twin 1a demonstrated extensive bilateral PVNH in the absence of any seizure disorder or developmental delay (Fig. 1). Twin 1b has yet to have an MRI of his brain performed. Through the use of a combination of direct sequencing and RT-PCR, both twins were shown to carry a de novo mutation in intron 15 of *FLNA*, c.2280+389T>A, which leads to the creation of an ectopic splice donor site. Use of this de novo donor splice site results in the inclusion of 74bp of intronic sequence into the *FLNA* transcript, resulting in a subsequent frameshift with premature termination of translation p.(Arg760fs*25). Transcripts with normal splicing were also detected in RNA samples from primary cells from twin 1a (Suppl. Fig. S3), indicating that the novel splice donor site was only selected in a subfraction of transcripts.

Case 2 has been previously described (Kapur, et al., 2010) (family 1) and is a member of a large kindred that segregates PVNH, CIPO and vascular anomalies (Fig. 1) The causative mutation has previously been shown to be a partial duplication of *FLNA* inclusive of intron 1 to exon 28. Further MLPA analysis suggests that the duplication extends to include exon 1 of

the neighbouring gene, *EMD* which lies 5' to *FLNA,* through to *FLNA* exon 26, with exon 29 showing normal copy number (Suppl. Fig S1).

Case 3 is from a large family segregating a CIPO-only phenotype in several males, with no phenotypic anomalies evident in obligate carrier females. The proband had a grossly dilated bowel noted at a 20-week gestation by ultrasound scan. Postnatally histological analysis of several colonic biopsies demonstrated normal numbers and appearance of ganglion cells, but diffuse abnormal layering of the circular and longitudinal muscularis propria of the ileum was present as previously described in other CIIPX cases (Fig. 1, Suppl. Fig. S1). No malrotation of the gut was observed. Direct sequencing of the exons and intron-exon boundaries of *FLNA* demonstrated that he was hemizygous for a 2 bp deletion, c.18_19delTC, which segregated with the phenotype in the family and is predicted to lead to a frameshift and premature truncation of protein translation, p.(Arg7Glyfs*98).

Two simplex cases were also studied with presentations of PVNH with variable extra-neuronal phenotypic features. Case 4 presented with seizures, bilateral PVNH, normal cognition and stature, mitral valve prolapse and thin, doughy skin. He reported no bowel symptoms. He was hemizygous for a maternally inherited missense mutation c.853C>T

p.(Arg285Cys). His mother, who was heterozygous for the same variant also had PVNH and seizures (Fig. 1).

Case 5, who presented with bilateral PVNH and joint hypermobility but no gastrointestinal symptoms, was shown to have a de novo variant in *FLNA*, c. 1065G>A, p.(Lys355Lys) (Fig. 1, Suppl. Fig. S1). This synonymous variant lies at the 3' end of exon 7 and therefore holds the potential to disrupt splicing and is not represented in online databases of genetic variants (ExAC, GnomAD). Using cDNA prepared from primary skin fibroblasts cultured in the presence and absence of cycloheximide, an agent that suppresses nonsense-mediated transcript decay, RT-PCR was performed using primers flanking the mutation site. In the presence of cycloheximide, several aberrant *FLNA* spliceforms in addition to retention of some normal spliceforms were detected (Suppl Fig. S3).

Case 6 is a female heterozygous for c.82A>G, p.(Met28Val), predicted to disrupt the putative ATG^{+82}. She presented with bilateral PVNH. Her mother, also a heterozygote for the same variant, has an identical presentation to her daughter.

3.2 FLNA expresses two protein isoforms differing at the N-terminus

To address the hypothesis that two discrete FLNA proteins, initiating at ATG^{+1} and ATG^{+82}, are encoded by the *FLNA* locus, we first studied a female (case 6) with a heterozygous missense variant c.82A>G; p.(Met28Val) that alters the second putative translation initiation codon (ATG^{+82}) in *FLNA.* We reasoned that if X chromosome inactivation was such that a substantial proportion of cells have inactivated the non-mutation bearing chromosome, any FLNA protein expressed from such cells must have initiated FLNA protein translation from an alternative initiation codon, most likely the 5' ATG initiation codon (ATG^{+1}). Under this hypothesis, cells expressing the non-mutant allele retain the potential to express *FLNA* from both initiator codons. X chromosome inactivation performed on blood leucocyte DNA using the *AR* assay (Allen, et al., 1992) demonstrated an allelic ratio of 64:36, enabling a comparison of FLNA abundance to be performed between these two groups of cells. In cultured skin fibroblasts obtained from case 6 we performed immunofluorescence using a validated antibody whose epitope detects all filamin A proteins and compared these data to fibroblasts obtained from healthy unrelated controls. Fibroblasts from case 6 exhibited two distinct cell populations as predicted by the ratio of X-chromosome inactivation, congruent with previous studies of individuals with PVNH and *FLNA* mutations (Reinstein, et al., 2013). Cell population 1 showed localization of FLNA with the actin cytoskeleton with signal intensity indistinguishable from controls. Cell population 2, while exhibiting typical FLNA distribution, had significantly lower FLNA abundance, consistent with this latter cell

population expressing the mutant *FLNA* allele (Fig. 2). Since the mutation substitutes the ATG^{+82} codon, this protein is likely to be the long isoform derived from the mutant allele, which lacks the downstream translation initiation site. Given the PVNH phenotype of Case 6, the data suggest the hypothesis that FLNA protein can be produced from an allele that lacks an ATG^{+82} initiation codon and are consistent with the existence of two FLNA protein isoforms which we denote as $FLNA^{+1}$ (a long isoform the translation of which begins from ATG^{+1}) and $FLNA^{+28}$ (a short isoform, initiating from ATG^{+82}).

3.3 CIPO in isolation is associated with loss of one FLNA isoform

To further test the hypothesis that two FLNA proteins with different N-termini are produced from the *FLNA* locus, a polyclonal antibody was raised in rabbits to a conjugated peptide representing the N-terminus of $FLNA^{+1}$ (αFLNA aa1-27). Its specificity was demonstrated in cells transfected with cloned constructs expressing the N-terminus of both $FLNA^{+1}$ and $FLNA^{+28}$ proteins (Suppl Fig. S2a). To directly test for the presence of endogenous $FLNA^{+1}$ protein, western blotting of whole cell lysates obtained from cultured fibroblasts was performed using both αFLNAaa1-27 and αMAB1678 antibodies, the latter of which detects total FLNA. Both antibodies detected FLNA protein indicating the presence of $FLNA^{+1}$ in control cells. Next, to test for evidence that $FLNA^{+1}$ can be produced independently of $FLNA^{+28}$, cell lysate from fibroblasts from case 3, who is predicted on the basis of the

position of his mutation to express the FLNA^{+28} isoform but lack the FLNA^{+1} isoform was subjected to the same analysis (Fig. 3a,b). These data demonstrated a lack of the FLNA^{+1} isoform but also that FLNA protein was still present, but only at 61% +/- 8% of the level observed in control cell lines. Under the assumption that there is no reciprocal up- or down-regulation of FLNA^{+28} in the presence of the mutation that precludes production of the FLNA^{+1} isoform, the fraction of total FLNA accounted for by the FLNA^{+1} isoform in control cells is estimated to be 39% +/- 8%. This ratio of FLNA isoforms in fibroblasts resembles the ratio calculated in this same cell type from Case 6 with the p.Met28Lys mutation using quantitative immunofluoresence (Fig. 2).

These data indicate that two discrete FLNA protein isoforms are translated in human fibroblasts. Furthermore, when considering the phenotypes observed in cases 3 and 6, these data suggest that a deficiency of the FLNA^{+1} isoform is linked to a CIPO outcome while deficiency of the FLNA^{+28} protein leads to PVNH. We therefore proceeded to study the protein levels of both isoforms in individuals with combinatorial CIPO/PVNH/vascular phenotypes (cases 1, 2) and males with PVNH alone (cases 4,5). Here, the hypothesis was that mutations that result in combined PVNH/CIPO presentations diminish both isoforms simultaneously. To address this hypothesis cell lines obtained from cases 1, 2, 4 and 5 were characterised by western analysis using antibodies specific for FLNA^{+1} and total FLNA (Fig. 3). Cases 1, 2, 4 and 5 showed variably reduced total FLNA, and large, significant reductions in

levels of FLNA^{+1} (Fig 3a-d). Interestingly in these cases, there is no clear correlation with the expression level of either total FLNA or FLNA^{+1} with clinical presentation.

From this experiment it can therefore be concluded that (a) while cases with complete loss of the FLNA^{+1} isoform consistently exhibit CIPO, no minimal threshold of FLNA^{+1} expression seems to accurately predict clinical outcome using the methodology used here and (b) mutations predicted to impair the production of both isoforms have the potential to produce combinatorial PVNH/CIPO/vascular phenotypes.

3.4 Low conservation of FLNA amino acids 1-27 suggests no structurally conserved function

Previously it has been suggested that the positions of the CIPO-alone phenotype mutations implicates the most N-terminal 28 amino acid residues as functionally important in intestinal function (Gargiulo, et al., 2007). To explore this hypothesis we sought indications that this sequence exhibits properties of conserved function by evaluating its evolutionary conservation. The FLNA protein as a whole shows high amino acid identity (85.2%) while the two hinge regions (hinge 1 and 2, which act as flexible linkers between the rod domains of FLNA) have relatively low conservation (65.3% and 57% respectively), a result also reflected in analysis of FLNA paralogs (van der Flier and Sonnenberg, 2001). Analysis of FLNA amino acids 1-27 (Fig. 3g) revealed low conservation (54.7%), suggesting that this region is unlikely

to be under structural constraint related to functional differences between the $FLNA^{+1}$ and $FLNA^{+28}$ isoforms.

3.5 CAGE RNA sequencing identifies the production of three differentially-regulated *FLNA* transcripts which correlate to intestinal and brain pathology

Having concluded that the *FLNA* locus produces two distinct protein isoforms, the question remains if they are produced from the same or distinct transcripts. Given the evidence derived from our study of case 3 that CIPO is caused by deficiency of the $FLNA^{+1}$ protein alone it is relevant to understand if this regulation is directed at the transcriptional or translational level. Furthermore, we failed, to replicate the findings of Garguilio et al. (Gargiulo, et al., 2007). These data raise the alternative possibility that the differential production of these separate FLNA protein isoforms is regulated at the transcriptional, rather than the translational, level. Mapping publicly available ESTs to the 5' end of *FLNA* suggests the existence of transcripts with different transcriptional start sites (TSS). Additionally, mapping of CAGE-tagged start sites using data pooled for all tissues and cell lines from the FANTOM database indicated the presence of several possible TSS, with the predominant site at position +28 bp 3' to ATG^{+1}. Two additional TSS locate to the 5' ends of exon 1 and 2 (Fig. 4a). These data indicate that *FLNA* produces multiple mRNA transcripts

that differ in their 5' regions and consequently may be differentially regulated to produce the $FLNA^{+1}$ and $FLNA^{+28}$ proteins.

As CIPO-alone phenotypes are caused by loss-of -function mutations 5' to ATG^{+82}, we next questioned if some of these transcripts are differentially regulated in ileal smooth muscle. To more comprehensively document *FLNA* TSS location and define tissue specific differences in their usage, CAGE RNA sequencing was undertaken from two control fibroblast cell lines and from micro-dissected smooth muscle from two ileal and two colonic samples. It was hypothesised that these intestinal tissues would demonstrate a bias for expression from TSS1 and/or TSS2, rendering FLNA expression insufficient in these cells when a pathogenic variant precludes their usage (case 3). The locations of TSS were defined and the relative expression level of their cognate transcripts quantified. Fibroblasts employ three TSS (Fig. 4b) each of similar amplitude, that correspond to the TSS observed in the mean pooled FANTOM database (Fig. 4a). The predicted transcripts include one that incorporates ATG^{+82} (TSS3) but not ATG^{+1},, while the other two transcripts begin at either the 5' end of exon 1 (TSS1) or 2 (TSS2), and contain both ATG^{+1} and ATG^{+82}.

The CAGE data on the intestinal tissue indicated a relative increase in employment of TSS1 of ~11 fold for colonic samples and ~8 fold for ileal samples compared to fibroblasts (Fig 4c,d) with a small increase in use of TSS2 and a reduction in TSS3 use . Further analysis of human fetal tissues extracted from the FANTOM CAGE data set indicated that, as with the

mean pooled FANTOM data, TSS3 is the predominant transcript in heart, kidney, liver and lung tissue (Fig. 4e). Interestingly, human fetal whole brain, occipital, parietal, and temporal lobe samples lack a signal for TSS1, while a small signal is detected for TSS2 (Fig. 4f), predicting that only low levels of $FLNA^{+1}$ protein is likely to be present in developing fetal brain tissue.

Collectively these CAGE data demonstrate differential use of the three TSS for *FLNA* and present a potential basis for the regulation of translation of different FLNA protein isoforms.

To substantiate this hypothesis it is necessary to associate the two FLNA protein isoforms with the three transcript isoforms (TSS1-3) characterised in this analysis. Consequently, V5-tagged *FLNA* minigenes were constructed with a 5'UTR corresponding to usage of TSS1, TSS2 and TSS3, with the latter construct only capable of initiating translation at ATG^{+82}. On western analysis using αFLNA aa1-27 and αV5 antibodies, clones incorporating TSS1 and TSS2 exclusively express only the $FLNA^{+1}$ isoform (Suppl. Fig. S2a) with no secondary bands associated with translational initiation from ATG^{+82}, contrary to previous observations (Gargiulo, et al., 2007). Moreover, when the truncating variant found in case 3 is inserted into a construct that otherwise has the capability to initiate translation at ATG^{+82} no $FLNA^{+28}$ is produced (Suppl. Fig. S2b), indicating that secondary initiation at this codon in mutation-bearing transcripts starting at TSS1/TSS2 is an unlikely explanation for the CIPO-alone phenotype observed in this individual.

These data clearly demonstrate that Ileal and colonic smooth muscle predominantly initiate transcription and upregulate *FLNA* at TSS1.

3.6 Gastrointestinal smooth muscle predominantly expresses the FLNA^{+1} protein isoform

To further correlate TSS usage with FLNA protein isoform production, we next performed western analysis on micro-dissected ileal smooth muscle samples (Fig. 3e,f). Leveraging from the conclusion (Figs. 2,3) that the FLNA^{+1} isoform constitutes ~36% of total fibroblast FLNA protein, we normalized the western signal obtained with the αFLNA 1-27 antibody to 36% of that obtained with the pan-FLNA antibody αMAB1687 in control fibroblasts and ileal and colonic smooth muscle samples. These data indicate that FLNA expression in ileal and colonic smooth muscle can be predominantly accounted for by the FLNA^{+1} isoform (Fig. 4f). While the CAGE data demonstrate an absolute level of expression of FLNA^{+28} in these tissues that is equivalent to that seen in fibroblasts, the significantly elevated (~10 fold) levels of FLNA^{+1} compared to fibroblasts results in this isoform being the predominant one in ileum and colon. Interestingly colonic smooth muscle also predominantly expresses FLNA^{+1} in a manner that is indistinguishable from ileum. These results are consistent with the immunohistochemical study of resected control colon; control samples stain strongly for

FLNA^{+1} in the circular and longitudinal muscularis externa, muscularia mucosa and in the vasculature of neonatal human colon (Fig 5a,c). In contrast in colonic sections obtained from Case 1b, no immunodetectable FLNA^{+1} was present (Fig. 5 b,d).

4 DISCUSSION

The phenotypic pleiotrophy associated with mutations in *FLNA* is amongst the most diverse for any locus in the human genome (Robertson, 2005). Loss-of-function mutations can result in combinations of periventricular nodular heterotopia (PVNH), congenital cardiovascular anomalies, CIPO and high rates of embryonic or fetal lethality, but the causal basis for these differences in presentation is unclear (Robertson, 2005; van der Werf, et al., 2012). In this study, we exploited the insights brought to light by the study of individuals with filaminopathy phenotypes. To begin to understand the genetic basis for some of this phenotypic diversity, we focused on the mutational spectrum leading to a myopathic intestinal dysmotility disorder, CIPO, which occurs exclusively in males. While CIPO occurs variably in association with other *FLNA* loss-of-function phenotypic features, in a subset of cases, CIPO is an isolated disorder.

Although the NCBI annotation of *FLNA* details a single TSS associated with production of a single protein isoform ($FLNA^{+1}$), the data presented here, including analysis of the FANTOM mean pooled CAGE dataset, reveal far more transcriptional complexity and indicate that the predominant TSS (TSS3) is 28 bp 3' from ATG^{+1}, where it sponsors translation initiation from the ATG^{+82} start site. Lacking however was data directly interrogating the usage of the two potential translation initiation start sites at a protein level. Immunofluorescence studies on fibroblasts from a female with a substitution at the canonical translation initiation start site (p.(Met28Val) confirmed two distinct cell populations, consistent with the production of two distinct FLNA protein isoforms, $FLNA^{+1}$ and $FLNA^{+28}$. Subsequent analysis of case 3, a male carrying the FLNA c.18_19delTC mutation that precludes production of the $FLNA^{+1}$ isoform, demonstrated directly that two protein isoforms ($FLNA^{+1}$:$FLNA^{+28}$) are expressed in fibroblasts in a ratio of ~1:1.8.

These studies indicated that individuals carrying mutations between the alternate translation initiation start sites retain expression of $FLNA^{+28}$, the deduction being that it is the loss of $FLNA^{+1}$ that is the key etiological factor producing the CIPO phenotype. Although it is conceivable that the differential regulation of the production of these two proteins could operate at the translational level, CAGE sequencing of fibroblast, ileal and colonic RNA clearly point towards a transcriptional basis for this observation with at least three identified TSSs, with TSS1 being the dominant isoform in gastrointestinal smooth muscle.

The mechanistic reason for switching reliance from TSS3 to TSS1 in intestinal smooth muscle is unclear, but it is less likely to relate to the novel 28aa N-terminus given its lack of evolutionary conservation and may relate more to the strength of the promoters associated with TSS1 compared to TSS3, since there is also a 10-fold increase in TSS1 transcript abundance in intestinal smooth muscle compared to that in skin fibroblasts. Altered ratios of FLNA to actin bestow dramatic changes to the actin cytoskeletal architecture that could possibly relate to its functions as a determinant of cell shape and mechanosensation (Nakamura, et al., 2014; Tseng, et al., 2004). Kapur et al (Kapur, et al., 2010) note that changes in small intestine smooth muscle shape are essential to the establishment of peristaltic action. Intestinal length, which is dramatically foreshortened in CIPO, is also probably related to the embryonic organisation of the muscularis propria, and may also influence intestinal rotation.

The data linking the FLNA^{+1} isoform to gut development also has a parallel in the regulation of FLNA in the fetal neuroepithelium, the cell type that is dysregulated to lead to PH, the canonical loss-of-function phenotypic characteristic in this group of disorders. FANTOM CAGE data indicate negligible use of TSS1, with the primary transcript being driven from TSS3, predicting a near exclusive dependence on the production of the FLNA^{+28} protein isoform in this tissue. This deduction is consistent with the PVNH phenotype in case 6 who

was heterozygous for a mutation that ablated the translation initiation start site for this isoform. Of note, residual low levels of translational initiation at p.Val28 seem an unlikely prospect since we have also ascertained an unrelated three-generation family with typical PVNH with a different missense mutation (p.Met28Lys) at this same codon.

Although it is clear that measurement of the two FLNA protein isoforms by western analysis cannot predict the presence or absence of CIPO in addition to PVNH when mutations occur more centrally in the *FLNA* gene body, these data do highlight some predictability for mutations occurring in exons 1 and 2 of *FLNA.* In aggregate, these data point to a key influence of the actin cytoskeleton in intestinal development and indicate the existence of unsuspected complexity in closely adjacent promoter elements at the *FLNA* locus.

Acknowledgements

The authors would like to thank the participants for their involvement in this research. SPR is supported by Curekids NZ.

Disclosure Statement

The authors declare no conflict of interest.

REFERENCES

Allen RC, Zoghbi HY, Moseley AB, Rosenblatt HM, Belmont JW. 1992. Methylation of HpaII and HhaI sites near the polymorphic CAG repeat in the human androgen-receptor gene correlates with X chromosome inactivation. American Journal of Human Genetics 51(6):1229-1239.

Antonucci A, Fronzoni L, Cogliandro L, Cogliandro R-FF, Caputo C, De Giorgio R, Pallotti F, Barbara G, Corinaldesi R, Stanghellini V. 2008. Chronic intestinal pseudo-obstruction. World journal of gastroenterology 14(19):2953-2961.

Auricchio A, Brancolini V, Casari G, Milla PJ, Smith VV, Devoto M, Ballabio A. 1996. The locus for a novel syndromic form of neuronal intestinal pseudoobstruction maps to Xq28. American journal of human genetics 58(4):743-748.

Berrou E, Adam F, Lebret M, Planche V, Fergelot P, Issertial O, Coupry I, Bordet JC, Nurden P, Bonneau D and others. 2017. Gain-of-Function Mutation in Filamin A Potentiates

Platelet Integrin alphaIIbbeta3 Activation. Arterioscler Thromb Vasc Biol 37(6):1087-1097.

Clayton-Smith J, Walters S, Hobson E, Burkitt-Wright E, Smith R, Toutain A, Amiel J, Lyonnet S, Mansour S, Fitzpatrick D and others. 2008. Xq28 duplication presenting with intestinal and bladder dysfunction and a distinctive facial appearance. European journal of human genetics : EJHG 17(4):434-443.

De Giorgio R, Cogliandro RF, Barbara G, Corinaldesi R, Stanghellini V. 2011. Chronic Intestinal Pseudo-Obstruction: Clinical Features, Diagnosis, and Therapy. Gastroenterology Clinics of North America 40(4):787-807.

Feng Y, Walsh CA. 2004. The many faces of filamin: a versatile molecular scaffold for cell motility and signalling. Nature cell biology 6(11):1034-1038.

Gargiulo A, Auricchio R, Barone MV, Cotugno G, Reardon W, Milla PJ, Ballabio A, Ciccodicola A, Auricchio A. 2007. Filamin A is mutated in X-linked chronic idiopathic intestinal pseudo-obstruction with central nervous system involvement. American journal of human genetics 80(4):751-758.

Guerrini R, Mei D, Sisodiya S, Sicca F, Harding B, Takahashi Y, Dorn T, Yoshida A, Campistol J, Kramer G and others. 2004. Germline and mosaic mutations of FLN1 in men with periventricular heterotopia. Neurology 63(1):51-6.

Haberle V, Forrest ARR, Hayashizaki Y, Carninci P, Lenhard B. 2015. CAGEr: precise TSS data retrieval and high-resolution promoterome mining for integrative analyses. Nucleic acids research 43(8).

Hehr U, Hehr A, Uyanik G, Phelan E, Winkler J, Reardon W. 2006. A filamin A splice mutation resulting in a syndrome of facial dysmorphism, periventricular nodular heterotopia, and severe constipation reminiscent of cerebro-fronto-facial syndrome. Journal of Medical Genetics 43(6):541-544.

Huelsmann S, Rintanen N, Sethi R, Brown NH, Ylänne J. 2016. Evidence for the mechanosensor function of filamin in tissue development. Scientific Reports 6:32798.

Kapur RP, Robertson SP, Hannibal MC, Finn LS, Morgan T, van Kogelenberg M, Loren DJ. 2010. Diffuse abnormal layering of small intestinal smooth muscle is present in patients with FLNA mutations and x-linked intestinal pseudo-obstruction. The American journal of surgical pathology 34(10):1528-1543.

Lad Y, Kiema T, Jiang P, Pentikäinen OT, Coles CH, Campbell ID, Calderwood DA, Ylänne J. 2007. Structure of three tandem filamin domains reveals auto-inhibition of ligand binding. The EMBO journal 26(17):3993-4004.

Liu J, Das M, Yang J, Ithychanda SS, Yakubenko VP, Plow EF, Qin J. 2015. Structural mechanism of integrin inactivation by filamin. Nature structural & molecular biology 22(5):383-389.

Machado FB RE, Radic CP, De Brasi CD, Medina-Acosta E. 2011. Identification of a highly polymorphic tetranucleotide repeat locus (DXpS) at Xp and development of a DXpS/HUMARA biplex methylation-based PCR assay that enhances detection of X-chromosome inactivation. Available from Nature Precedings <http://dx.doi.org/10.1038/npre.2011.6633.1> (2011).

Nakamura F, Song M, Hartwig JH, Stossel TP. 2014. Documentation and localization of force-mediated filamin A domain perturbations in moving cells. Nature communications 5:4656.

Oda H, Sato T, Kunishima S, Nakagawa K, Izawa K, Hiejima E, Kawai T, Yasumi T, Doi H, Katamura K and others. 2016. Exon skipping causes atypical phenotypes associated with a loss-of-function mutation in FLNA by restoring its protein function. European journal of human genetics : EJHG 24(3):408-414.

Oegema R, Hulst JM, Theuns-Valks SD, van Unen LM, Schot R, Mancini GM, Schipper ME, de Wit MC, Sibbles BJ, de Coo IF and others. 2013. Novel no-stop FLNA mutation causes multi-organ involvement in males. American journal of medical genetics. Part A 161A(9):2376-2384.

Parrini E, Ramazzotti A, Dobyns WB, Mei D, Moro F, Veggiotti P, Marini C, Brilstra EH, Dalla Bernardina B, Goodwin L and others. 2006. Periventricular heterotopia: phenotypic heterogeneity and correlation with Filamin A mutations. Brain : a journal of neurology 129(Pt 7):1892-1906.

Popowicz GM, Schleicher M, Noegel AA, Holak TA. 2006. Filamins: promiscuous organizers of the cytoskeleton. Trends in biochemical sciences 31(7):411-419.

Reinstein E, Frentz S, Morgan T, García-Miñaúr S, Leventer RJ, McGillivray G, Pariani M, van der Steen A, Pope M, Holder-Espinasse M and others. 2013. Vascular and connective tissue anomalies associated with X-linked periventricular heterotopia due to mutations in Filamin A. European journal of human genetics : EJHG 21(5):494-502.

Robertson SP. 2005. Filamin A: phenotypic diversity. Current opinion in genetics & development 15(3):301-307.

Robertson SP, Twigg SR, Sutherland-Smith AJ, Biancalana V, Gorlin RJ, Horn D, Kenwrick SJ, Kim CA, Morava E, Newbury-Ecob R and others. 2003. Localized mutations in the gene encoding the cytoskeletal protein filamin A cause diverse malformations in humans. Nature genetics 33(4):487-491.

Royer P, Ricour C, Nihoul-Fekete C, Pellerin D. 1974. [The familial syndrome of short small intestine with intestinal malrotation and hypertrophic stenosis of the pylorus in infants]. Arch Fr Pediatr 31(2):223-9.

Schmoller KM, Lieleg O, Bausch AR. 2009. Structural and viscoelastic properties of actin/filamin networks: cross-linked versus bundled networks. Biophysical journal 97(1):83-89.

Sheen VL, Dixon PH, Fox JW, Hong SE, Kinton L, Sisodiya SM, Duncan JS, Dubeau F, Scheffer IE, Schachter SC and others. 2001. Mutations in the X-linked filamin 1 gene cause periventricular nodular heterotopia in males as well as in females. Hum Mol Genet 10(17):1775-83.

Tseng Y, An KM, Esue O, Wirtz D. 2004. The bimodal role of filamin in controlling the architecture and mechanics of F-actin networks. The Journal of biological chemistry 279(3):1819-1826.

van der Flier A, Sonnenberg A. 2001. Structural and functional aspects of filamins. Biochimica et biophysica acta 1538(2-3):99-117.

van der Werf CS, Sribudiani Y, Verheij JBGM, Carroll M, O'Loughlin E, Chen C-H, Brooks AS, Liszewski KM, Atkinson JP, Hofstra RMW. 2012. Congenital short bowel syndrome as the presenting symptom in male patients with FLNA mutations. Genetics in medicine : official journal of the American College of Medical Genetics 15(4):310-313.

FIGURE LEGENDS

Figure 1

Clinical and MRI images from individuals with PH, (indicated by arrows) with associated pedigrees.

(A) A de novo mutation in Case 1 and his twin brother, with MRI indicating bilateral PH; (B) Case 2 pedigree and ileum histology exhibiting disordered layering of smooth muscle, previously reported in (Kapur, et al., 2010); (C) Pedigree containing case 3 showing carrier females and affected males with a histological section of ileum from case 3, showing similar presentation of disordered smooth muscle; (D) Pedigree containing case 4 with MRI exhibiting PH; (E) Case 5 bearing a de-novo mutation, with MRI showing PH: (F) Case 6 (a female) with MRI exhibiting PH. Yellow arrows: Periventricular nodular heterotopia.

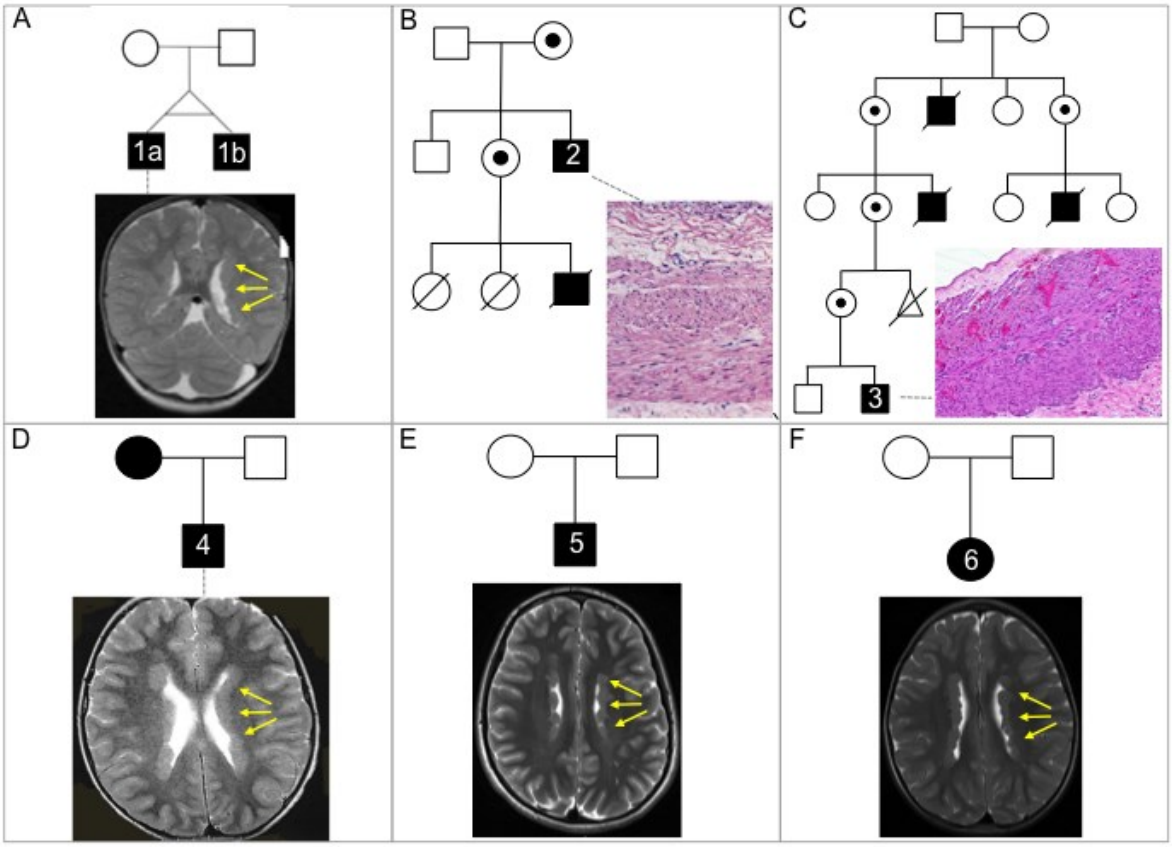

Figure 2

Alternate usage of translation initiation start sites at ATG^{+1} and ATG^{+82} in case 6 fibroblast cell line.

(A) Schematic view of 5'UTR of *FLNA* (NM_001456.3), encompassing exons 1 and 2, the second of which contains the annotated translation initiation site at position ATG^{+1}, and the second predicted site at position ATG^{+82} (ENST00000369856.7). The position of variant (c.82A>G) in case 6 that alters ATG^{+82} is noted above the sequence with an asterisk; (B) Immunofluoresence of primary fibroblast cell line of female case, probed with anti-FLNA MAB1678 (green), anti-GAPDH (red) and counter stained with DAPI. Two cell populations with differential intensity of FLNA staining are observed, one staining more faintly (arrows). (C) Relative quantitation of individual cellular expression of FLNA in case 6 and two female control cell lines using Fiji image analysis software. Data was normalized to GAPDH signal and background staining (n=50 for all cell lines). Results are expressed as relative intensity of FLNA immunofluorescence.

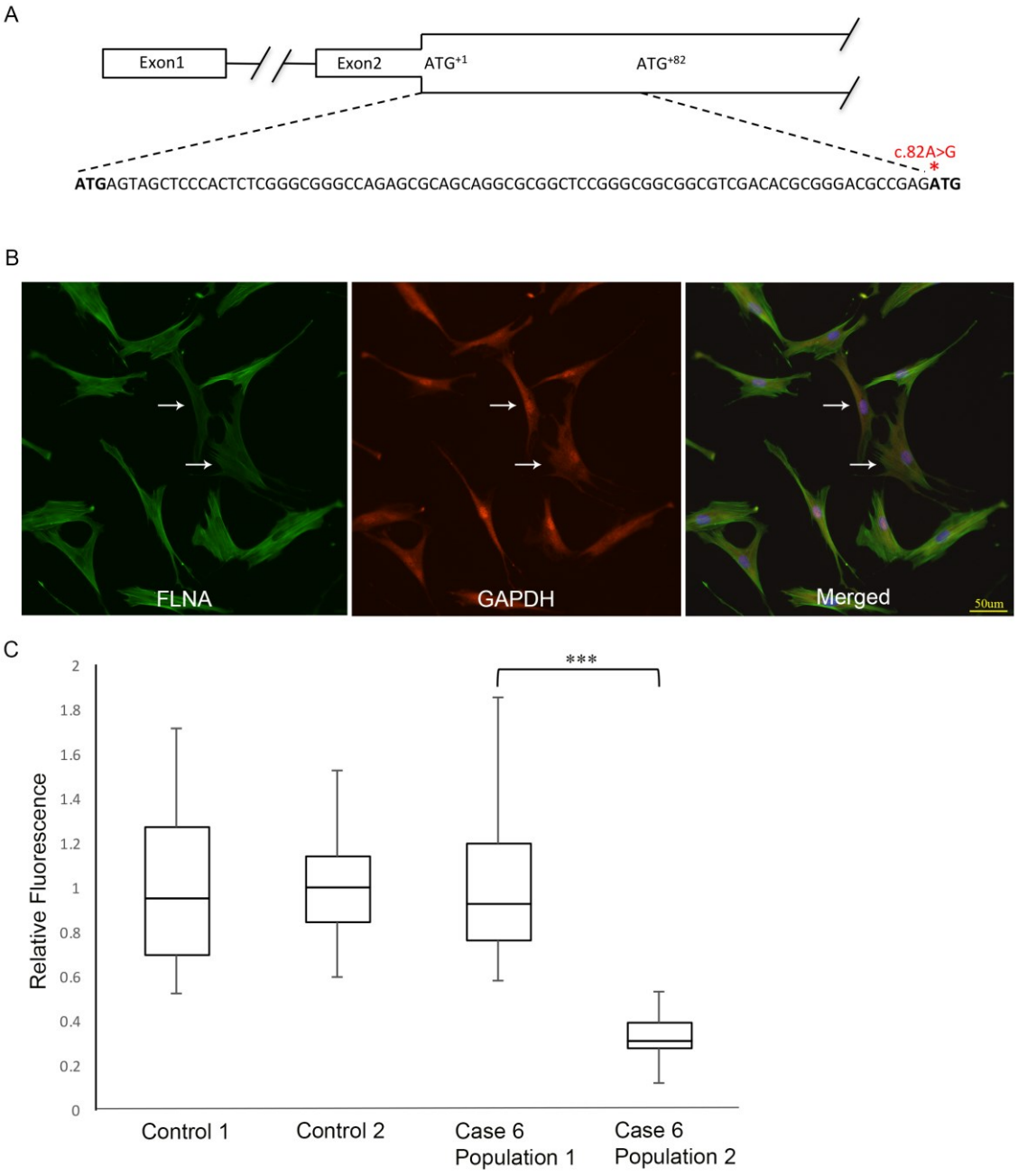

Figure 3

Loss or reduced expression of FLNA isoforms in case cell lines.

(A) Three control and case fibroblast cell lines were analysed by western analysis (n=3) and probed with anti-FLNAaa1-27 (specifically detecting the $FLNA^{+1}$ protein isoform), or anti-MAB1678 (detecting total FLNA). Samples were normalized to GAPDH signal. (B) Quantitation of relative FLNA isoform abundance expressed relative to pooled control samples, with asterix indicating statistical significance compared to control samples by T-test. Cases exhibiting CIPO are indicated; (C,D) Two control and two case EBV transformed lymphoblast cells lines probed and for FLNA isoform expression and quantitation/statistical analysis, as for fibroblast cell lines (n=3). (E) Quantitation by western analysis of FLNA isoforms in ileal and colonic smooth muscle. (F) $FLNA^{+1}$ expression normalized to a ratio of $FLNA^{+1}$:total FLNA of 1:1.8 in fibroblast samples. (G) Homology alignment of FLNA amino acids preceding the second putative initiator methionine (M^{+28}) using MegAlign™ version 9.1. DNASTAR. Madison, WI. Amino acid key; Red denotes small, hydrophobic and aromatic amino acids excluding tyrosine. Blue denotes acidic amino acids. Magenta denotes basic amino acids excluding histidine. Grey denotes other amino/imino acids.

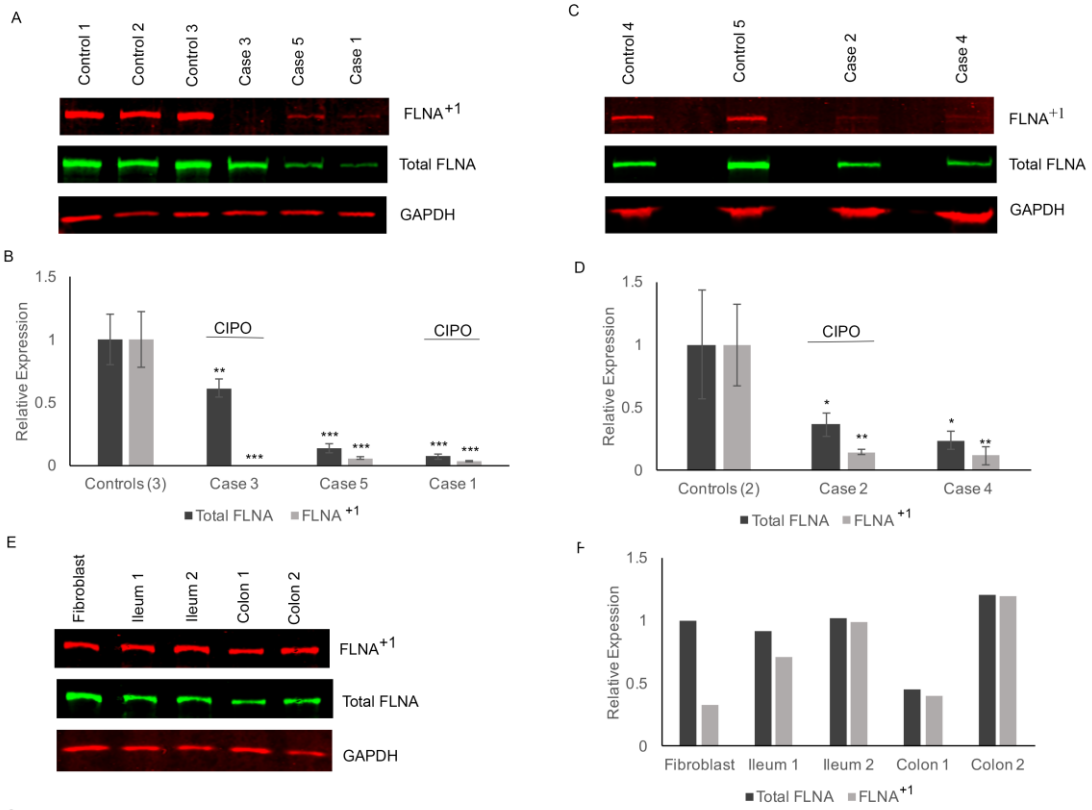

G

```
Homo sapiens          MSSSHSRAGQSAAGAAPGGG--VDTRDAE
Mus musculus          MSSSHSRCGQSAAVASPGGS--IDSRDAE
Canis lupus           MSSSHSRAGQSAAGAAPGGG--ADTRDAE
Bos taurus            MSSSHSRAGQSAAGAVLGIG--ADTRDAE
Danio rerio           MS-QHTRPHQSSAAAPLSNASLSPDKDAD
Xenopus tropicalis    MSSAHSRLSTQSGGA--GGA--VPGEAAE
Gallus gallus         MS-AAGRARE------------P--EAE
                      **    *                  *
```

Figure 4

Histogram of CAGE defined transcription start sites (CTSS) for the 5' region of *FLNA* (nucleotides 1-332bp ; NM_001110556.1).

(A) Histogram of FANTOM5 CAGE Phase 1 CTSS pooled mean count values for all tissues/samples in the data set, aligned with a schematic of the *FLNA* exons 1 and 2, depicting relative usage and expression level of alternate TSS clusters. (B-D) Histograms of pooled mean CTSS count values from two fibroblast cell lines, and two ileal and colonic micro-dissected smooth muscle biopsy samples across the same region. Peaks indicated by brackets depict calculated TSS clusters, here defined as TSS1, TSS2 and TSS3: (E) Human fetal tissue panel and (F) human fetal brain data extracted from FANTOM5 STAR showing total CTSS count values at TSS1, TSS2 and TSS3.

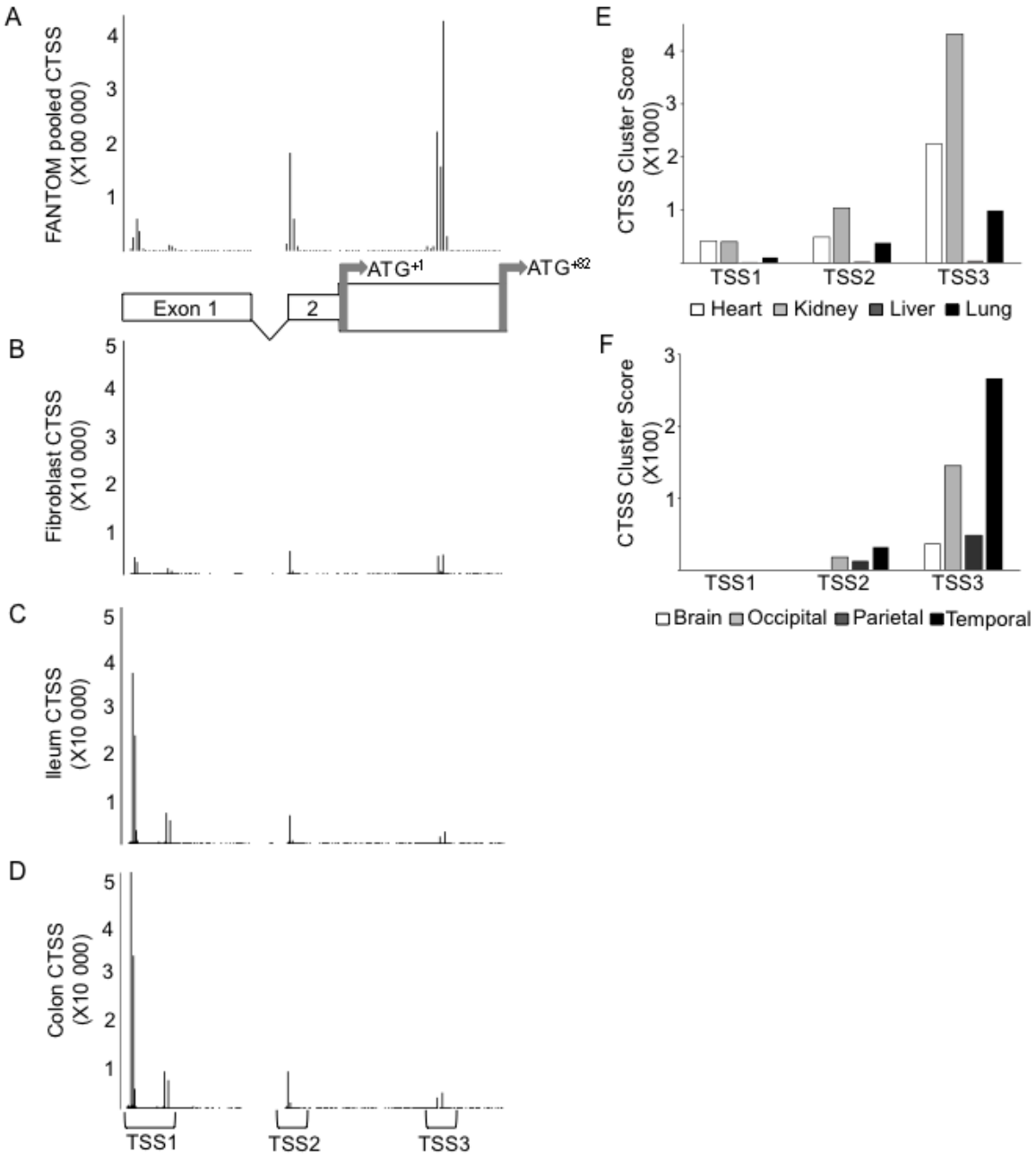

Figure 5

Immunohistochemical staining using αFLNA aa1-27 and total FLNA on fixed sections of colon from control and case 1b.

Staining with anti-FLNA aa1-27, images of control sample (A) showing strong staining in longitudinal and circular muscularis propria, and muscularis mucosa layers in addition to vascular elements. Comparison with case 1b (B) shows no detectable $FLNA^{+1}$ staining. Staining of total FLNA with anti-FLNA (Sigma HPA001115) in control (C) and case 1b (D) colon respectively, showing comparable staining with anti-FLNA aa1.27.

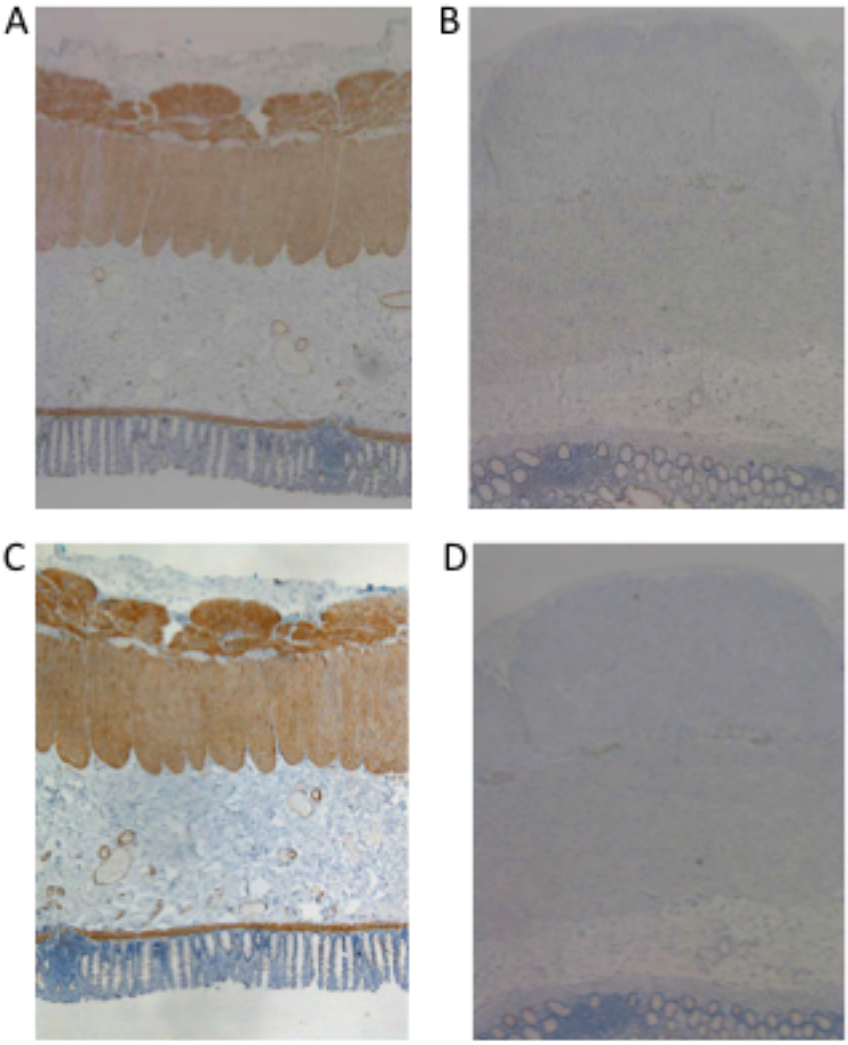

Table 1. Case phenotypes, mutations and predicted effects on protein isoforms

	Age	Sex	Nucleotide ATG^{+1}	Nucleotide ATG^{+82}	Predicted Protein FLNA^{+1}	Predicted Protein FLNA^{+28}	Phenotype
1	8	M	c.2280+389T>A	c.2199+389T>A	p.(Arg760fs*25)	p.(Arg733fs*25)	CIPO, PVNH, bronchiectasis
2	24	M	g.(EMD ex1)_(FLNA ex26) dup	g.(EMD ex1)_(FLNA ex26) dup	?	?	CIPO, PVNH
3	8	M	c.18_19del	c.1-62_63del	p.(Arg7Ffs*98)	unaffected	CIPO
4	17	M	c. 853C>T	c.772C>T	p.(Arg285Cys)	p.(Arg258Cys)	PVNH, atrial septal defect, prolapsed mitral valve, joint laxity, translucent skin
5	22	M	c.1065G>A	c.984G>A	p.(Lys355lys)	p.(Lys328Lys)	PVNH, joint laxity, translucent skin
6	17	F	c.82A>G	c.1A>G	p.(Met28Val)	p.(Met1Val)	PVNH

PVNH, periventricular nodular heterotopia; CIPO congenital intestinal pseudo-obstruction; EMD, gene encoding emerin; M, male; F, female